MECOM99
Mendoza
6-10 de septiembre de 1999

COMPUTATIONAL FRACTURE ANALYSES BY MEANS OF VIRTUAL CRACK CLOSURE INTEGRAL METHODS

Friedrich-G. Buchholz, Azzedine Chergui, Hans A. Richard
Institute of Applied Mechanics, University of Paderborn
D-33098 Paderborn, Germany

ABSTRACT

In this paper the capability of Virtual Crack Closure Integral (VCCI) methods regarding the computational fracture analysis of 2D and 3D crack problems is presented. For the 2D case the accuracy and convergence is verified on the basis of a reference solution for the CCT specimen and in comparison to other methods. In the 3D cases emphasis is on the analysis of mixed mode problems involving also local 3D and different mode coupling effects, in particular where a crack front intersects a free surface. It can be stated that the MVCCI results agree very well with the global behaviour of the reference solutions but also remarkable deviations are found where mode coupling effects seem not to be covered by the solutions available from stress analysis handbooks or the literature so far.

INTRODUCTION

The understanding and analysis of mixed mode fracture is an important subject in fracture mechanics because material flaws or pre-cracks, which may have been introduced unintentionally during the manufacturing processes, can have an arbitrary orientation with respect to a general type of loading which a component of a machine or structure has to carry.

In the past, 2D crack extension problems under mixed mode I and II loading conditions have attracted much attention and through many investigations the problem is now well understood. A number of fracture criteria for predicting the onset of fracture and the direction of crack growth under mixed mode I and II crack tip loading conditions are well established (Erdogan and Sih[1]; Williams and Ewing[2]; Sih[3]; Hussain, Pu and Underwood[4]; Nuismer[5]; Wu[6]; Palaniswamy and Knauss[7]; Cotterell and Rice[8]; Sumi, Nemat-Naser and Keer[9]; Amestoy, Bui and Dang-Vam[10]; Leblond and Amestoy[11]). In particular, the compact tension shear (CTS) specimen designed by Richard[12] in combination with the special loading device (Richard and Benitz[13]) and detailed experimental and computational investigations have contributed to the current state in the field (Banks-Sills, Arcan and Bui[14]; Richard[15]).

In this paper the capability of Virtual Crack Closure Integral (VCCI) methods regarding the computational fracture analysis of 2D and 3D crack problems is presented. For the 2D case the accuracy and convergence is verified on the basis of a reference solution for the CCT specimen and in comparison to other methods.

Furthermore, detailed results of 3D finite element and mixed mode analyses of four different types of fracture specimens are presented and discussed. Special interest is taken in local 3D and mode coupling effects to be found in stress intensity factor (SIF) or strain energy release rate (SERR) results along crack fronts, in particular adjacent to an intersection of a crack front with a free surface of the specimen. The four specimens under consideration are a centre cracked tension (CCT) specimen, with a crack perpendicular or inclined to the loading direction, a single edge notched (SEN) specimen under out-of-plane shear, a quarter circular corner crack (QCCC) specimen subject to shear and a three point bending (3PB) specimen with a crack perpendicular or inclined with respect to the mid plane between the supports (see Fig.1 and Tab.1). The specimens and loading conditions have been chosen to suit

the subject of this investigation and such that reference solutions are available from stress analysis handbooks or the literature (Tada, Paris and Irwin[16]; Rooke and Cartwright[17]; Murakami[18]; Isida[19]; Pook[20]).

Moreover, some experimental findings are presented, showing the influence of variable mixed mode loading conditions along the crack front on the development of 3D crack extension in the 3PB specimen with an angled crack.

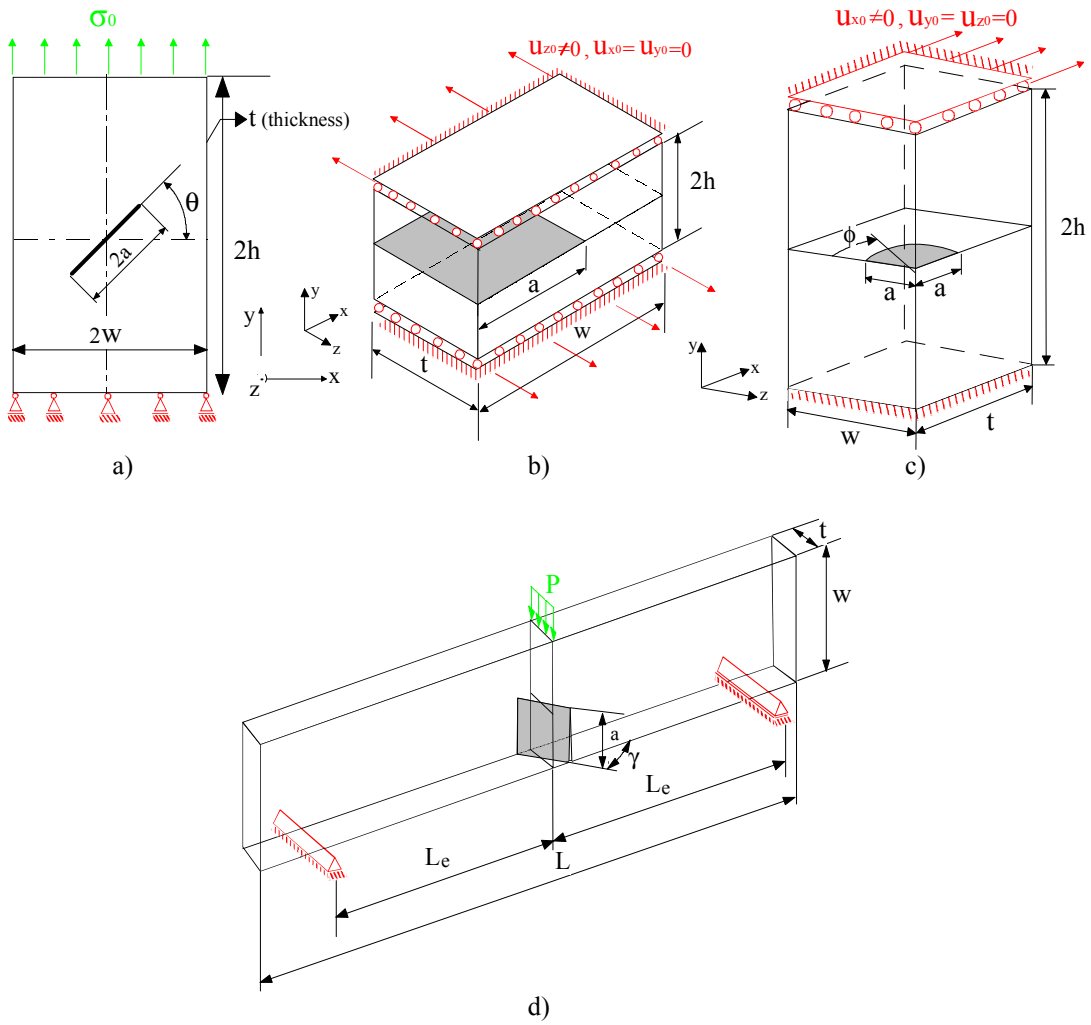

Figure 1: Specimen types and loading conditions
a) CCT-specimen b) SEN-specimen
c) QCCC-specimen d) 3PB-specimen

	CCT-spec.	SEN-spec.	QCCC-spec.	3PB-spec.
Lenght L_e (mm)	-	-	-	120
Height h (mm)	48	25	100	-
Width w (mm)	24	100	100	60
Thickness t (mm)	12	50	100	20
a/w (-)	0.5	0.5	0.4	0.3
Angle (deg.)	0; 45	-	-	45; 90

Table 1: Geometrical parameters of the specimens

2D AND 3D VIRTUAL CRACK CLOSURE INTEGRAL (VCCI) METHODS

VCCI or 2C Method

With reference to Fig.2 and its notations for mode I crack tip conditions, Irwin's[21] well known analytical crack closure integral relation is given by

$$G_I(a) = \lim_{\delta a \to 0} \frac{2}{\delta a} \int_{x=0}^{x=\delta a} \frac{1}{2} \sigma_{yy}(r = x, \phi = 0, a)\, u_y(r = \delta a - x, \phi = \pi, a + \delta a)\, dx. \tag{1}$$

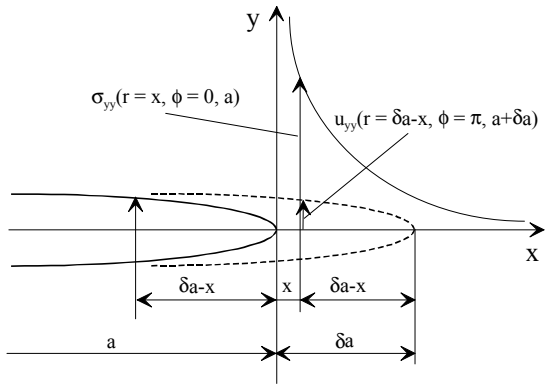

Figure 2: Analytical VCCI method

For the FE analysis of the related crack problem Eq.(1) can be written in the following FE representation

$$G_I^{2C}\left(a + \frac{\Delta a}{2}\right) = \frac{1}{t\Delta a} W^y, \qquad W^y = \frac{1}{2} F_{y,i}(a) \cdot \Delta u_{y,j-1}(a + \Delta a) \tag{2}$$

which is holding for a FE discretisation as given in Fig.3a. By Eq.(2), in which t denotes the thickness of the specimen, the SERR G_I is calculated on the basis of the work to be done by the nodal point force $F_{y,i}(a)$ against the relative nodal point displacement $\Delta u_{y,j-1}(a + \Delta a)$ in order to close the crack by Δa again (Fig.3a). By Eq.(2) the numerical VCCI method is defined for a 2D crack problem under mode I. In this paper it will be shown that through this method, which can be classified as a local energy approach, good results are obtained even for non-singular, low order standard elements and rather coarse FE meshes, if the layout of the mesh around the crack tip is homogeneous.

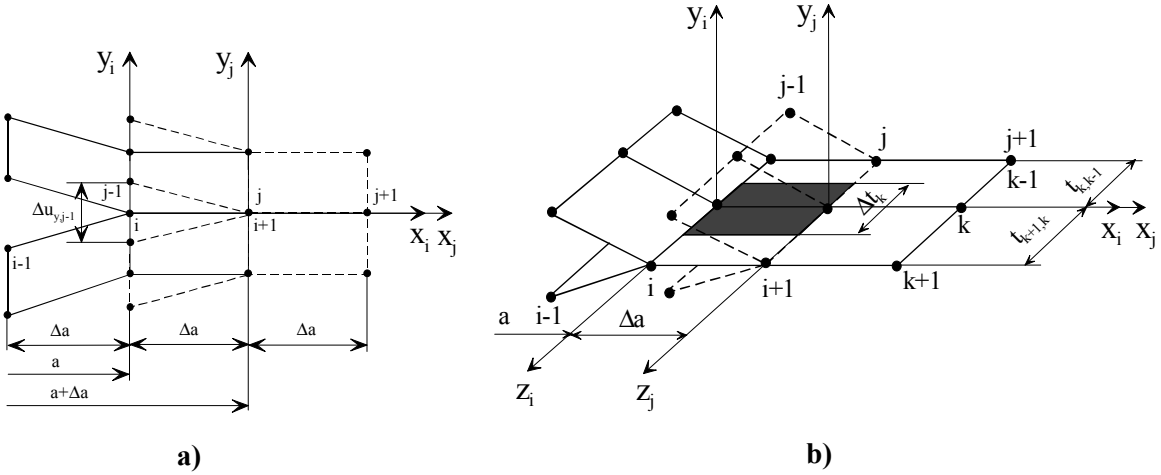

Figure 3: Computational VCCI methods for 2D and 3D low order element discretisations
a) 3- and 4-node membrane or b) 6- and 8-node volume elements

Here the VCCI method is also named and marked as 2C method (2 calculations), because two FE analyses of the model have to be performed, respectively (for the crack lengths a and $a + \Delta a$), in order to compute one SERR result $G^{2C}(a + \Delta a/2)$ as mean value in the interval of finite crack extension Δa. But with respect to this effort it should be emphasised that by Eq.(2) the SERR is computed numerically exact for the actual FE discretisation under consideration, even for finite crack extensions $\Delta a >> 0$. On that account no term $\lim\Delta a \to 0$ is expressed in Eq.(2) and the notation $G^{2C}(a + \Delta a/2)$ stresses its meaning as the mean value of the SERR in the interval Δa of finite crack extension (from crack length a to $a + \Delta a$), which has to be correlated to $a + \Delta a/2$, the corresponding mean value of the crack length in the interval under consideration.

MVCCI or 1C Method

Rybicki and Kanninen[23] have introduced the modified virtual crack closure integral (MVCCI) method in order to avoid the additional effort of a second FE analysis for an extended crack of length $a + \Delta a$, respectively. This can be achieved if, with reference to Eq.(2) and to Fig.3a, the required relative nodal point displacement $\Delta u_{y,j-1}(a+\Delta a)$ from the extended crack is replaced by the corresponding relative nodal point displacement $\Delta u_{y,i-1}(a)$ of the original crack with crack length a. By this numerically highly effective MVCCI or 1C method (1 calculation) the SERR is calculated from

$$G_I^{1C}(a) = \lim_{\Delta a \to 0} \frac{1}{t\Delta a} W^y, \qquad W^y = \frac{1}{2} F_{y,i}(a) \Delta u_{y,i-1}(a). \tag{3}$$

The assumptions under which Eq.(3) is holding are the same as for Eq.(2). Through the term $\lim\Delta a \to 0$ in Eq.(3) it is expressed that the MVCCI or 1C method is an approximate approach, with convergence to the exact solution (Eq.(1)) only for $\Delta a \to 0$. But Rybicki and Kanninen[23] have shown, that for small Δa also a good accuracy with respect to reference solutions can be achieved by the MVCCI method.

In the case of in-plane mixed mode loading conditions at the crack tip or in the 3D case including out-of-plane shear the additional mode II or mode III SERRs can be obtained readily by substituting the relevant x- and z-components of the nodal point forces and the relative nodal point displacements into Eq.(3). The total SERR at the crack tip or at a nodal point located along the crack front is then defined by

$$G_T^{1C}(a) = \sum_{\mathrm{i}} \mathrm{G}_{\mathrm{i}}^{1\mathrm{C}}(a), \qquad \mathrm{i} = \mathrm{I}, \mathrm{II} \quad \text{or} \quad \mathrm{i} = \mathrm{I}, \mathrm{II}, \mathrm{III}. \tag{4}$$

This numerically highly effective MVCCI method for 2D fracture analysis can be generalised in conjunction with low order volume element discretisations in a rather straight forward way in order to cover also complex 3D fracture problems. Firstly Eqs.(2)-(4) have to be evaluated at all nodal point positions k =1, 2... along the crack front (Fig.3b) and they have to be interpreted there with respect to a locally defined crack front coordinate system, respectively. Secondly the constant thickness t at the 2D problems has to be replaced by an effective thickness Δt_k, which is correlated to the nodal point position k under consideration and evaluation (Fig.3b). The resulting formulae are

$$G_I^{1C}(a, \Delta t_k)_{\mathrm{k}} = \lim_{\Delta a \to 0} \frac{1}{\Delta \mathrm{t}_{\mathrm{k}} \Delta a} W_k^y, \qquad W_k^y = \frac{1}{2}\left(F_{y,i}(a) \Delta u_{y,i-1}(a)\right)_k, \tag{5a}$$

$$G_{II}^{1C}(a, \Delta t_k)_{\mathrm{k}} = \lim_{\Delta a \to 0} \frac{1}{\Delta \mathrm{t}_{\mathrm{k}} \Delta a} W_k^x, \qquad W_k^x = \frac{1}{2}\left(F_{x,i}(a) \Delta u_{x,i-1}(a)\right)_k, \tag{5b}$$

$$G_{III}^{1C}(a, \Delta t_k)_{\mathrm{k}} = \lim_{\Delta a \to 0} \frac{1}{\Delta \mathrm{t}_{\mathrm{k}} \Delta a} W_k^z, \qquad W_k^z = \frac{1}{2}\left(F_{z,i}(a) \Delta u_{z,i-1}(a)\right)_k, \tag{5c}$$

$$\Delta \mathrm{t}_{\mathrm{k}} = \frac{t_{k,k-1} + t_{k+1,k}}{2}, \tag{5d}$$

which are holding for 6- and 8-node volume element discretisations (Fig.3b). In the following it will be shown that also in the 3D case through this method, which again can be classified as a local energy approach, good results are obtained even for non-singular, low order standard elements and rather coarse FE meshes, if the layout of the mesh around the crack front is homogeneous.

The corresponding formulae for the VCCI-method for 3D crack problems can readily be developed from Eq.(2) and Eqs.(5a,b,c), respectively.

Through further generalisations of the method, also the numerically more effective non-singular, higher order elements can be utilised for the fracture analysis of 2D and 3D crack problems (Buchhholz[24]; Krishnamurthy et al[25]: Raju[26]; Sethuraman and Maiti[27]; Buchholz et al[28,29]; Narayana et al[30]; Shivakumar, Tan and Newman[31]; Buchholz[32]) and also other methods have been developed (Chan, Tuba and Wilson[33]; Parks[34]; Hellen[35]; Kuna[36]; Nikishkov and Atluri[37]; Mi and Aliabadi[38]; Wawrzynek et al[39]; Dhondt[40,41]).

OTHER METHODS OF COMPUTATIONAL FRACTURE ANALYSIS

Global Energy Method

According to Irwin[22] the change of the total elastic potential $\Pi(a)$ due to a crack extension from length a to a+Δa in an elastic solid is related to the total SERR $G_T(a)$ by

$$G_T(a) = -\lim_{\Delta a \to 0} \frac{\Pi(a+\Delta a) - \Pi(a)}{t\Delta a} = -\frac{d\Pi(a)}{td(a)} \tag{6}$$

(t = const., thickness of the solid). The total elastic potential is defined as

$$\Pi(a) = U(a) - W^E(a) \tag{7}$$

with

$$W^E(a) = \underline{U}(a)^T \underline{F} \tag{8}$$

and

$$U(a) = \frac{1}{2}\underline{U}(a)^T \underline{\underline{K}}\, \underline{U}(a) \tag{9}$$

denoting the elastic potential of the applied loads and the elastic strain energy of the solid, respectively ($\underline{U}$ displacement vector, $\underline{F}$ load vector, $\underline{\underline{K}}$ stiffness matrix of the solid, respectively).

For a finite crack extension Δa in the FE model of a cracked solid the global energy method EN2 is given by

$$G_T^{EN2}\left(a + \frac{\Delta a}{2}\right) = -\frac{\Pi(a+\Delta a) - \Pi(a)}{t\Delta a}, \tag{10}$$

and through

$$G_T^{EN3}(a) = -\frac{\Pi(a+\Delta a) - \Pi(a-\Delta a)}{t2\Delta a} \tag{11}$$

the global energy method EN3 is established. Based on computational experience with different FE codes, FE discretisations and element types, Eqs.(10) and (11) will give reliable and accurate results for the total SERR as long as the crack is modelled in a homogeneous FE mesh (see Figs.5 and 6) and furthermore, Δa is chosen reasonably large in order to avoid extreme small numbers for $\Delta\Pi$ and reasonably small to avoid a poor FE modelling of the crack. On the other hand the global energy methods EN2 and EN3 have the disadvantage that the total SERR can not be decomposed into separated SERRs $G_i(a)$, i=I,II, although these are of high importance for all mixed mode fracture problems. Nevertheless, the global energy methods are very useful for cross-checking the

accuracy of other methods of computational fracture analysis, like the local energy methods VCCI and MVCCI, by which the total SERR $G_T(a)$ is calculated through the separated modes $G_i(a)$, i=I,II or i=I,II,III by Eq.(4).

Extrapolation Method

In order to verify the performance of the local and global energy methods, they will be compared with one of the classical methods of computational fracture analysis. Here the displacement extrapolation method DE180 is chosen, because through computational experience it is known, that by this method generally a better accuracy is achieved, compared to the alternative stress extrapolation method SE000, which is based on the singular stress field at the crack tip (Fig.2, φ=0). In case of mode I the DE180 method is based on the crack tip displacement field

$$\begin{pmatrix} u_x(r,\varphi) \\ u_y(r,\varphi) \end{pmatrix} = K_I \sqrt{\frac{r}{2\pi}} \frac{1+\nu}{E} (\kappa - \cos\varphi) \begin{pmatrix} \cos\frac{\varphi}{2} \\ \sin\frac{\varphi}{2} \end{pmatrix} \tag{12}$$

(Fig.2, $\varphi=\pi$) and the mode I SIF is given by

$$K_I = \lim_{r\to 0} \sqrt{\frac{2\pi}{r}} \frac{E}{(1+\nu)(\kappa+1)} u_y(r,\varphi=\pi), \qquad \kappa = \begin{cases} \frac{3-\nu}{1+\nu} & \text{plane stress} \\ 3-4\nu & \text{plane strain} \end{cases}. \tag{13}$$

Through Irwin's[21] analytical virtual crack closure relations (for i=I see Eq.(1)) the SERRs G_i are related to the SIFs K_i by

$$G_i = \frac{K_i^2}{E'}, \qquad i = I, II \qquad \text{with} \qquad E' = \begin{cases} E & \text{for plane stress} \\ \frac{E}{1-\nu^2} & \text{for plane strain} \end{cases} \tag{14}$$

and

$$G_{III} = (1+\nu)\frac{K_{III}^2}{E}. \tag{15}$$

DISCUSSION OF RESULTS

Accuracy and Convergence

In order to test and verify the accuracy and convergence of the local energy methods VCCI and MVCCI, compared to the global energy method EN3 and the displacement extrapolation method DE180, the CCT specimen Fig.4 is considered because for this problem a detailed reference solution is available. Due to the symmetry of the problem only one quarter of the specimen has to be modelled (Fig.4).

The three different FE meshes C, M and F under investigation are shown in Fig.5. They are characterised by increasing mesh refinements adjacent to the crack and a homogeneous mesh along the crack line, respectively. In Fig.6 the deformed FE meshes C and F of the specimen are plotted from the analysis with 4-node quadrilateral elements, respectively.

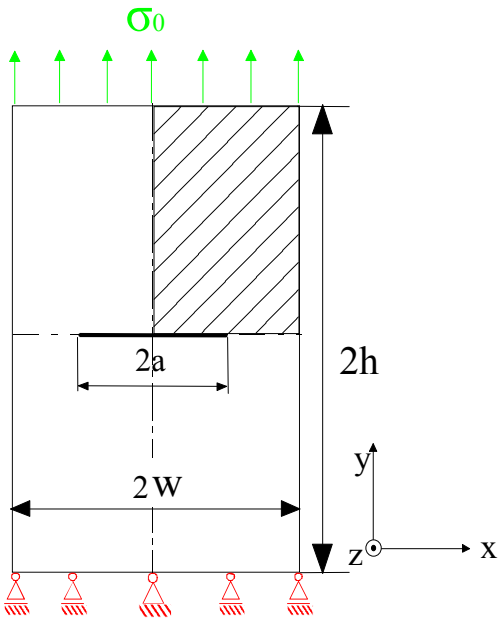

Figure 4: CCT specimen as a 2D problem with a reference solution (Isida[19])
(a/w=0.5, h/w=2, w=24mm)

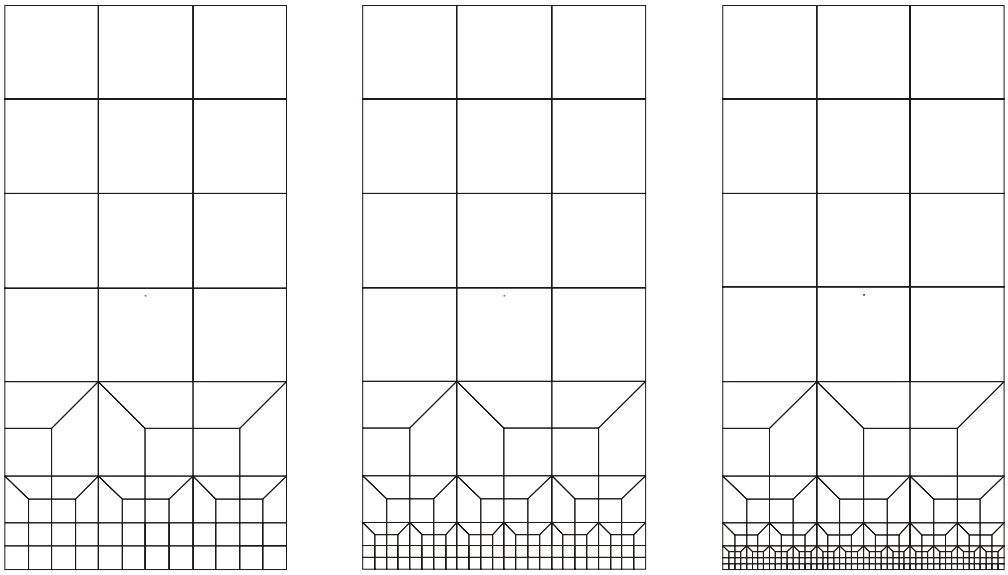

Coarse mesh C	**Medium mesh M**	**Fine mesh F**
w/Δa=12	w/Δa=24	w/Δa=48
Δa/a=0.167	Δa/a=0.083	Δa/a=0.042
Δa=2mm	Δa=1mm	Δa=0.5mm

Figure 5: FE meshes of the CCT specimen (one quarter) with homogeneous mesh refinement along the crack line
(4-node quadrilateral elements)

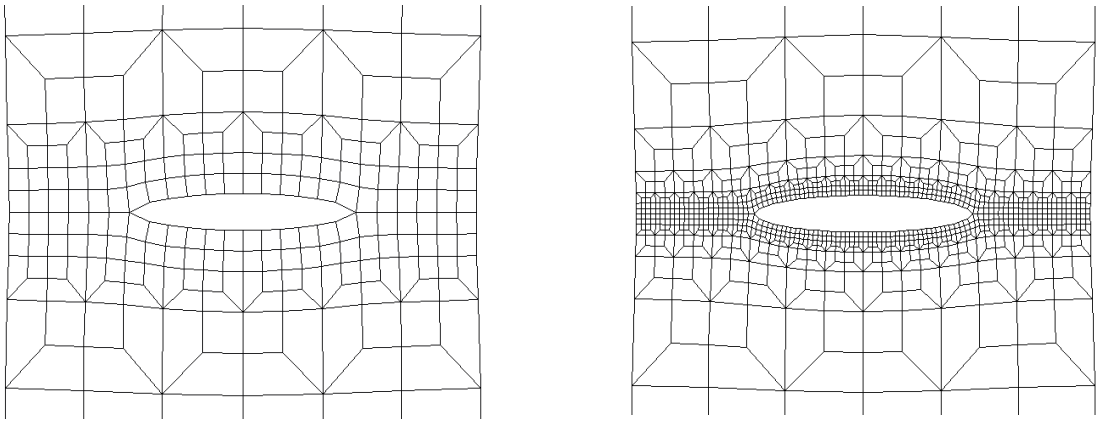

Figure 6: Deformed meshes C and F of the CCT specimen
(4-node quadrilateral elements)

The quantitative results for the normalised SIFs, computed by the different methods for the meshes C,M and F, are plotted in Fig.7, together with the reference value (Isida[19]). It can be seen that the results for the global energy method EN3 and the local energy method VCCI coincide for all meshes and with increasing mesh refinement also the small deviations of the MVCCI results disappear. For the larger deviations of the DE180 method this is not observed, but with further mesh refinement, compared to mesh F, convergence can also be expected. Based on Eq.(13) the extrapolation procedure for the DE180 method is shown in Fig.8 for the meshes C, M and F. For $r/a<0.4$ increasing deviations from the extrapolation lines are found for all meshes, confirming that the strong gradients of the crack tip fields can not be modelled accurately by low order standard elements, like the 4-node quadrilateral elements under consideration. But still the relative error $\Delta rel=-3.20\%$ for the DE 180 method and mesh F is acceptable and so is $\Delta rel=-2.19\%$ for the other methods and mesh F, as given in Tab.2. If a higher accuracy is desired or required, this can be achieved easily through further mesh refinements or by choosing higher order standard elements (e. g. 8-node quadrilateral elements) for the same meshes C, M and F. In this case $\Delta rel<-1\%$ is found for all methods, already for mesh M, and $\Delta rel<-0.5\%$ for mesh F, respectively.

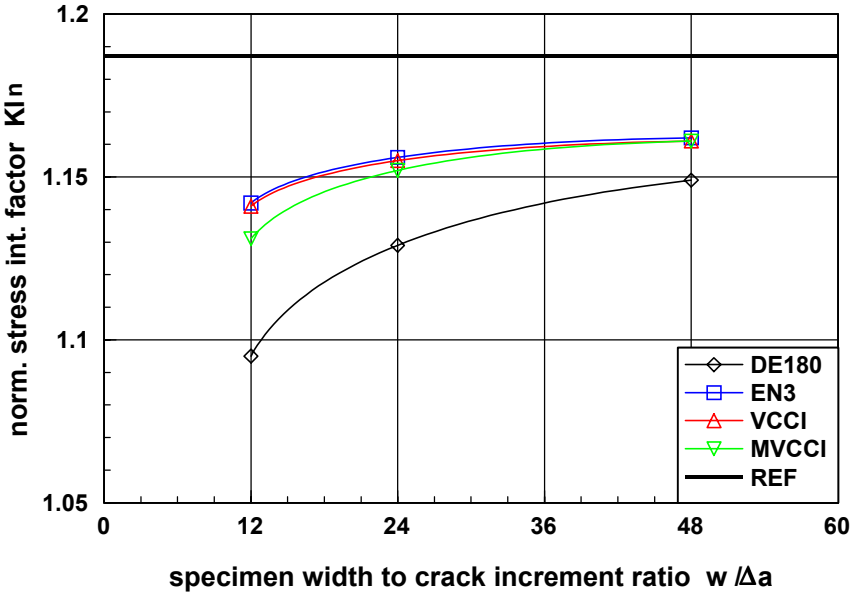

Figure 7: Accuracy of norm. SIFs computed by diff. methods with 4-node quad. elements and meshes C, M, F
(FE-code ABAQUS)

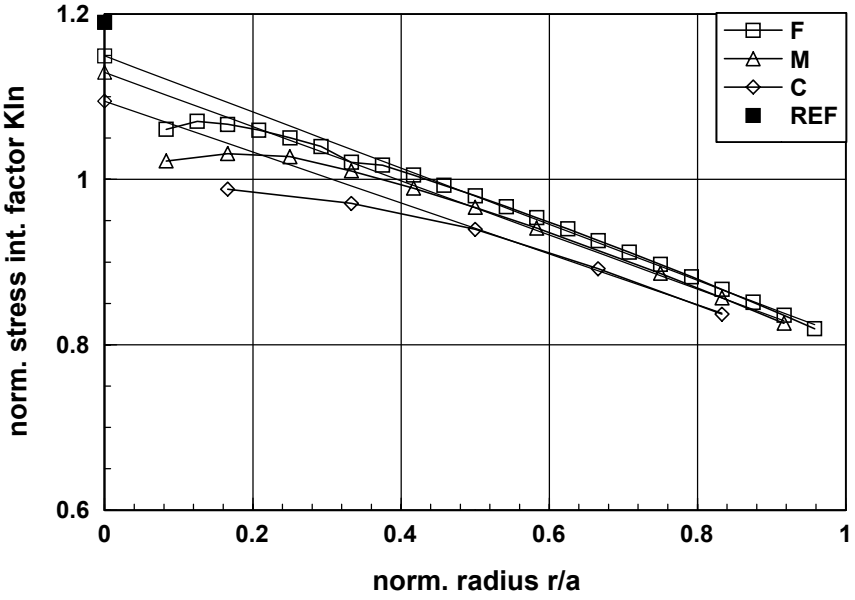

Figure 8: Accuracy of norm. SIFs computed by DE180 method with 4-node quad. elements and meshes C, M, F (FE-code ABAQUS)

l/w=2.0						
a/w=0.5						
KIn-ref=1.187						
mesh	**C** **w/Δa=12** **a/Δa=0.167**		**M** **w/Δa=24** **a/Δa=0.083**		**F** **w/Δa=48** **a/Δa=0.042**	
method	**KIn**	**Δrel %**	**KIn**	**Δrel %**	**KIn**	**Δ rel %**
DE180	1.095	-7.75	1.129	-4.89	1.149	-3.20
EN3	1.141	-3.88	1.155	-2.70	1.161	-2.19
VCCI (2C)	1.141	-3.88	1.155	-2.70	1.161	-2.19
MVCCI (1C)	1.131	-4.72	1.152	-2.95	1.161	-2.19

Table 2: Accuracy of norm. SIFs computed by diff. methods with 4-node quad. elements and meshes C, M, F (FE-code ABAQUS)

Based on the presented results the global and local energy methods EN3 and VCCI and MVCCI have achieved the best accuracy for all meshes C, M and F under consideration. But the local energy methods have the advantage of delivering the separated SERRs $G_i(a)$, i = I, II in the mixed mode cases. Because by the MVCCI or 1C method (1 calculation) this is achieved by just one analysis of the FE model, this method is computationally most effective and thus has been chosen for the following fracture analyses of different 3D problems, involving mixed mode loading conditions and also different 3D and mode coupling effects.

Centre cracked tension (CCT) specimen

Also for the 3D problems the investigation begins by considering the CCT-specimen first, in order to test the MVCCI method regarding the correlated 3D FE model (Fig.9) and to verify its computational accuracy concerning the low order standard elements that have been chosen (8-node volume elements). Also for the 3D model of the CCT specimen this can be confirmed based on the results given in Fig.10 and in Tab.3, although for the 3D case no reference solution is available. The way how to relate the results of the 3D model of the CCT specimen to the 2D reference solution is to suppress all displacements in the thickness direction of the specimen (z- or 3-direction, see

Fig.9) by setting $u_{z0}(x,y,z/t=\pm 0.5)=0$ as boundary conditions (BCs) at the front and rear surface of the specimen (1,2-planes). By this trick plane strain conditions are enforced on the 3D model of the CCT specimen. In consequence these surfaces of the deformed specimen remain plane, even at crack front intersections. (see the corresponding mesh detail in Fig.9), and the SERRs evaluated along the crack front through the thickness of the specimen should be constant and related to the corresponding 2D reference value (Isida[19]). In order to find a common basis for the comparison of the results the SERRs calculated by the MVCCI method are converted into SIFs by the aid of Eq.(14) for i=I, II and by Eq.(15) for i=III. This finally results in the normalised SIFs as plotted in Fig.10 and given quantitatively in Tab.3. They are found to be perfectly constant along the crack front and through the small relative error of Δrel=-1.60 %, compared to the 2D plane strain reference value (Tab.3), this 3D FE model of the CCT specimen and the 3D generalisation of the MVCCI method can be assessed as qualified for the analysis of more general 3D cases.

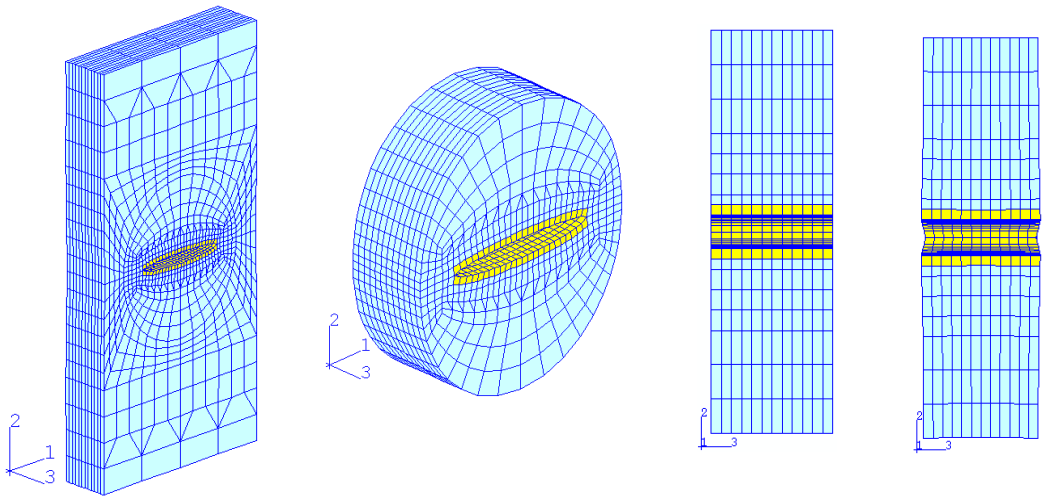

Figure 9: Deformed 3D FE model of the CCT specimen (θ=0 deg.) and crack details with/without pl. strain BCs in thickness direction
(6- and 8-node vol. el., w/Δa=24, Δa/a=0.083, Δt/t=0.083, Δa=Δt=Δh=1mm)

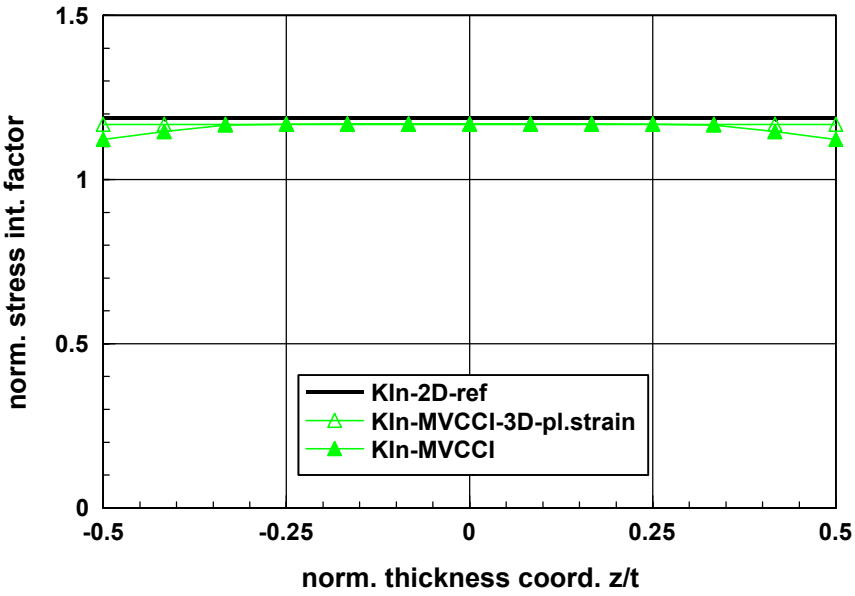

Figure 10: Norm. SIFs along the crack front of the CCT specimen with/without pl. strain BCs in thickness direction

For the real 3D analysis of the CCT specimen the K_{In} values are found to be nearly constant along the crack front in the inner part of the specimen (-0.25<z/t<0.25), but show slightly decreasing values where the crack front meets the free surfaces of the specimen (z/t→±0.5), see Fig.10. This behaviour is well known and is related to the laterally less constrained strains there and results in the surface displacements clearly to be recognised in the corresponding mesh detail in Fig.9. Certainly the slightly curved and convex crack fronts, which are found in most mode I fatigue experiments, are correlated to this 3D effect through reduced fatigue crack growth rates for z/t→±0.5.

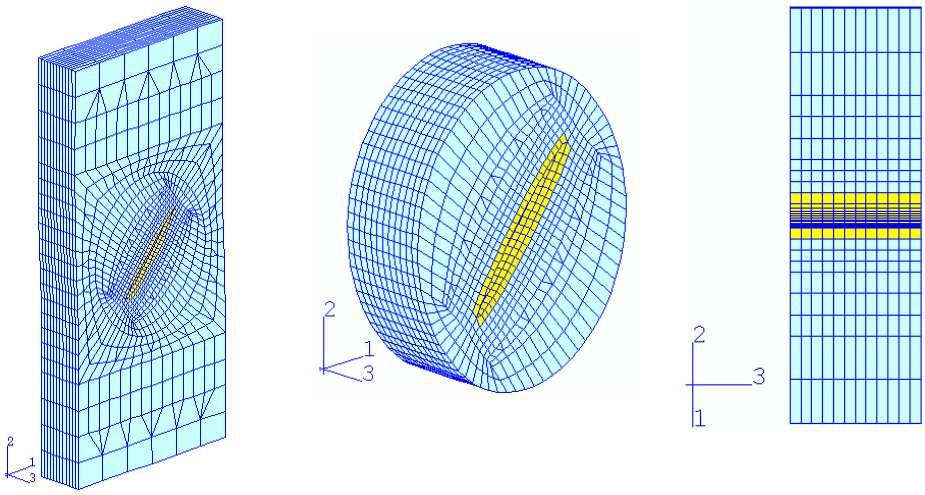

Figure 11: Deformed 3D FE model of the CCT specimen (θ=45 deg.) and crack details with pl. strain BCs in thickness direction
(6- and 8-node vol. el., w/Δa=24, Δa/a=0.083, Δt/t=0.083, Δa=Δt=Δh=1mm)

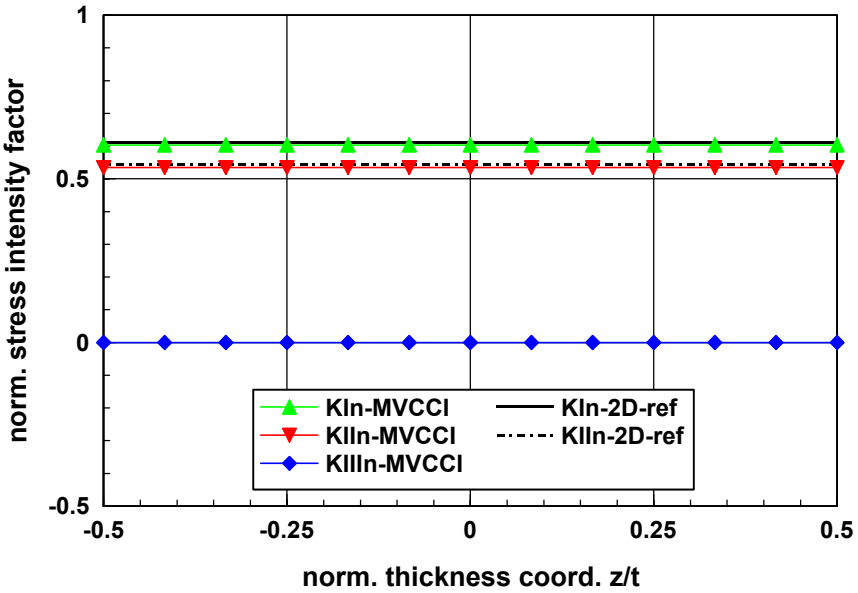

Figure 12: Norm. SIFs along the crack front of the CCT spec. (θ=45 deg.) with pl. strain BCs in thickness direction

Secondly an inclined crack in a 3D FE model of the CCT specimen (Figs.1a and 11) is analysed. In this case mode I and mode II loading conditions are generated at the crack tip by the unidirectional tension loading of the specimen and for the 2D case this problem is also thoroughly investigated and documented (Murakami[18]). Again we can refer to these data, by enforcing plane strain BCs to the corresponding 3D model of the specimen (Fig.11). Also for this in-plane mixed mode case the norm. SIF values $K_{In}(a,z/t)$ and $K_{IIn}(a,z/t)$ are perfectly const. along the crack front

through the thickness of the specimen (Fig.12) and the small relative errors of –1.42% and –2.12%, respectively (see Tab.3), with respect to the 2D plane strain reference solution (Murakami[18]), confirm again the accuracy of the FE model and the MVCCI method.

Finally the 3D model of the CCT specimen is analysed without enforcing plane strain boundary conditions. For this real 3D problem no reference solution is available, but since the thickness of the specimen is rather small (t=12mm, Tab.1) the 2D reference values should still be applicable. Inside the specimen for -0.4<z/t<0.4 this is confirmed by Fig.14 and Tab.3, but adjacent to the locations, where the crack front intersects the free surfaces of the specimen (z/t=±0.5), some minor 3D effects are found. A slight decrease in $K_{In}(a,z/t)$ is analysed for z/t→±0.5 and a slightly more pronounced increase in $K_{IIn}(a,z/t)$ is found, which means that the 2D results are no more conservative through this local 3D effect. But furthermore the 3D analysis shows that also mode III loading conditions are ensued along the crack front, although the external loading of the CCT-specimen obviously does not contain an out-of-plane shear component.

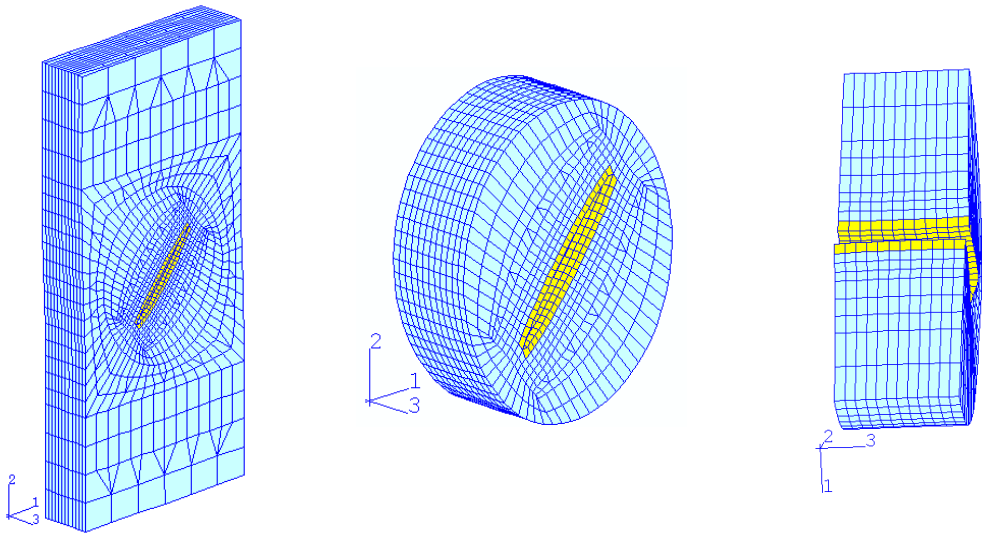

Figure 13: Deformed 3D FE model of the CCT specimen (θ=45 deg.) and crack details (6- and 8-node vol. el., w/Δa=24, Δa/a=0.083, Δt/t=0.083, Δa=Δt=Δh=1mm)

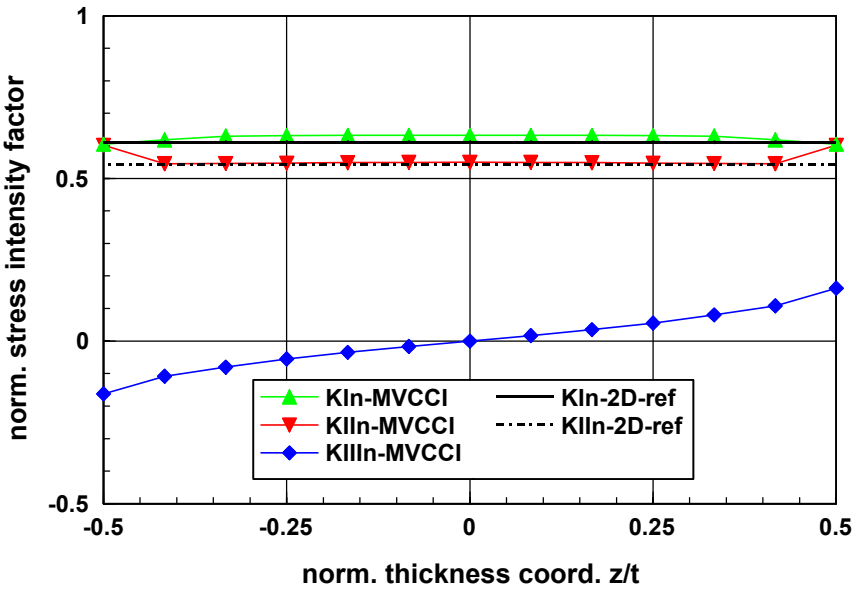

Figure 14: Norm. SIFs along the crack front of the CCT specimen (θ=45 deg.)

Here the mode III loading conditions along the crack front are due to a mode coupling effect between the mode II loading component of the specimen (due to the inclined crack) and mode III. This coupling effect is related to Poisson's ratio and the laterally less constrained strains adjacent to the free surfaces of the specimen. Consequently in Fig.14 $K_{IIIn}(a,z/t)$ vanishes for the mid plane of the specimen ($z/t=0$) and shows increasing values of opposite sign for $-0.4<z/t<0.4$ and higher gradients for $z/t\rightarrow\pm0.5$, where the crack front intersects the free surfaces of the specimen. The correlated surface displacements can clearly be recognised in the mesh detail of Fig.13 (displacement magnification factor 30). They are induced by the mode II loading component of the crack through the Poison's ratio effect. Based on the computational fracture analysis results of the CCT specimen presented and discussed above it finally can be stated, that, with respect to the fairly coarse mesh and the standard 8 node volume elements for the FE-model under consideration, the accuracy of the method, as documented in Figs.10, 12 and 14 and Tab.3, is very promising for the analysis of the following 3D mixed mode problems.

FE-model	method	KIn	KIn-ref	Δrel	KIIn	KIIn-ref	Δrel
3D θ=0 deg (pl. strain BC)	**MVCCI**	1.168	1.187	-1.60 %	-	-	-
3D θ=0 deg (at z/t=0)	**MVCCI**	1.169	-	-	-	-	-
3D θ=45 deg (pl. strain BC)	**MVCCI**	0.6032	0.6119	-1.42 %	0.5342	0.5458	-2.12 %
3D θ=45 deg (at z/t=0)	**MVCCI**	0,6320	-	-	0.5493	-	-

Table 3: Normalised SIF results for the CCT specimen and reference values

Single edge notched (SEN) specimen

The second specimen under consideration is the SEN specimen subject to out-of–plane shear loading through prescribed displacements as shown in Fig.1b. From the axonometric and the top view of the FE model (Fig.15) the global mode III deformation of the specimen as well as its local deformation at $z/t=0.5$ can be clearly recognised. In the inner part of the specimen for $-0.3<z/t<0.3$ the computational results for $K_{IIIn}(a,z/t)$, see Fig.16, agree very well with the reference solution (Murakami[18]). However, for $|z/t|>0.3$ the reference values K_{IIIn}-ref$(a,z/t)$ decrease continuously to zero, whereas from the MVCCI method $K_{IIIn}(a,z/t)>0$ is found, which seems to be in agreement with the distinct local mode III deformation to be observed at the crack tip for $z/t=0.5$ in Fig15.

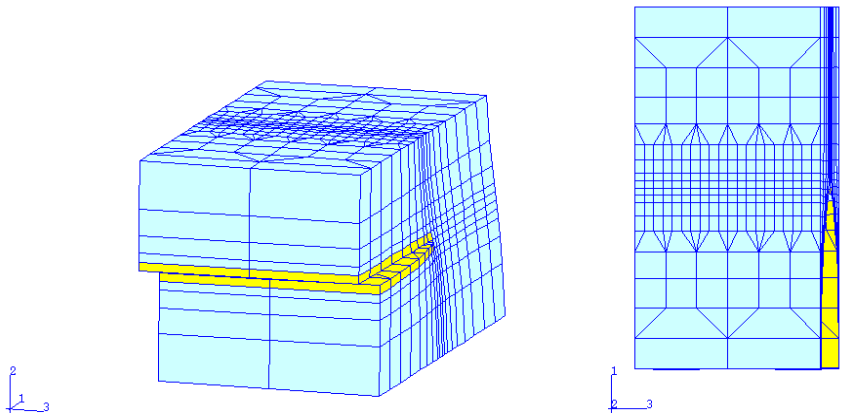

Figure 15: Deformed FE model of the SEN specimen under out-of-plane shear loading (6- and 8-node vol. el., $w/\Delta a=100$, $\Delta a/a=0.02$, $\Delta t/t=0.02$, $\Delta a=\Delta t=\Delta h=1$mm)

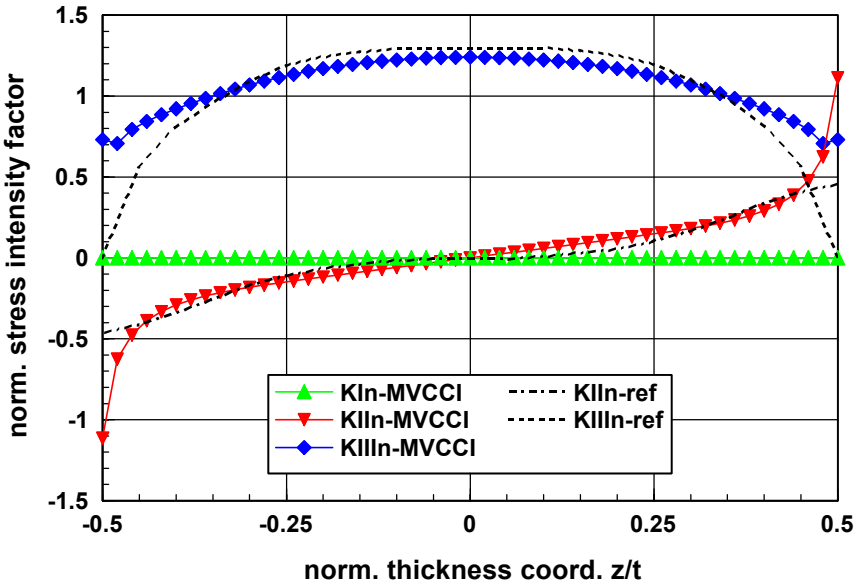

Figure 16: Norm. SIFs along the crack front of the SEN specimen under out-of-plane shear loading

Furthermore, in Fig.16 remarkable mode II conditions along the crack front are analysed by the MVCCI method and the reference solution, although the specimen is subject to pure out-of-plane shear displacements. Consequently, in the SEN specimen a strong mode coupling effect from mode III to mode II is effective, which mainly seems to be due to the global deformation behaviour of the specimen under the applied out-of-plane shear loading. But the strong gradients found for $K_{IIn}(a,z/t)$ for $z/t \rightarrow \pm 0.5$ by the MVCCI method seem to be induced by the mode III loading of the crack front adjacent to the free surfaces of the specimen and the Poisson's ratio effect.

Quarter circular corner crack (QCCC) specimen

The third specimen type to be investigated here is the QCCC specimen, which differs from the other specimens through the curved crack front. The specimen is loaded in shear by prescribed displacements, as given in Fig.1c, such that along the quarter circular crack the loading conditions could be expected to vary continuously from mode III, for the crack front position $\Phi/(\pi/2)=0$, to mode II for $\Phi/(\pi/2)=1$ (Fig.1c). However, the situation is more complex as can be seen from the results given in Fig.18. For $\Phi/(\pi/2)=0$ not only mode III is acting due to the external shear loading of the specimen, but also mode II of about the same magnitude and for $\Phi/(\pi/2)=1$ not only mode II is acting due to the shear loading, but also a considerable mode III portion. In Fig.17 this can also be recognised at the deformed FE model of the QCCC specimen and more pronounced, at the crack surface detail by the local dislocations of the crack tip meshes at both crack front positions, respectively. This means that at both crack front edges mode coupling takes place, mode II induced by mode III for $\Phi/(\pi/2) \rightarrow 0$ and mode III induced by mode II for $\Phi/(\pi/2) \rightarrow 1$. Here the mode coupling seems to be caused by a combination of the global deformation behaviour of the specimen and Poisson´s ratio effects.

On the other hand, the overall behaviour of the MVCCI results is similar as in the previous case, where along the inner part of the crack front the computational results agree well with the reference solution (Murakami[18]) and adjacent to the crack front intersections with the free surfaces of the specimen distinct deviations are found, respectively. But it should be mentioned here, that all the MVCCI results presented in this paper for the four different specimens under consideration have recently been strongly confirmed (Buchholz, Chergui, Dhondt[42]) by findings from another approach, based on a different modelling technique (Dhondt[41]) and utilising singular quarter point volume elements (Dhondt[40]).

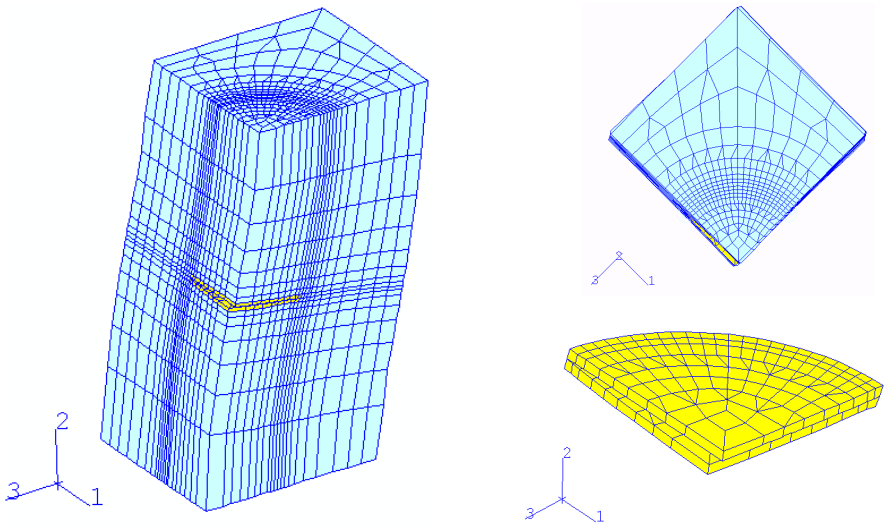

Figure 17: Deformed FE model of the QCCC specimen under shear loading and crack surface details (6- and 8-node vol. el., w/Δa=38.2, Δa/a=0.065, Δt/(aπ/2)=0.042)

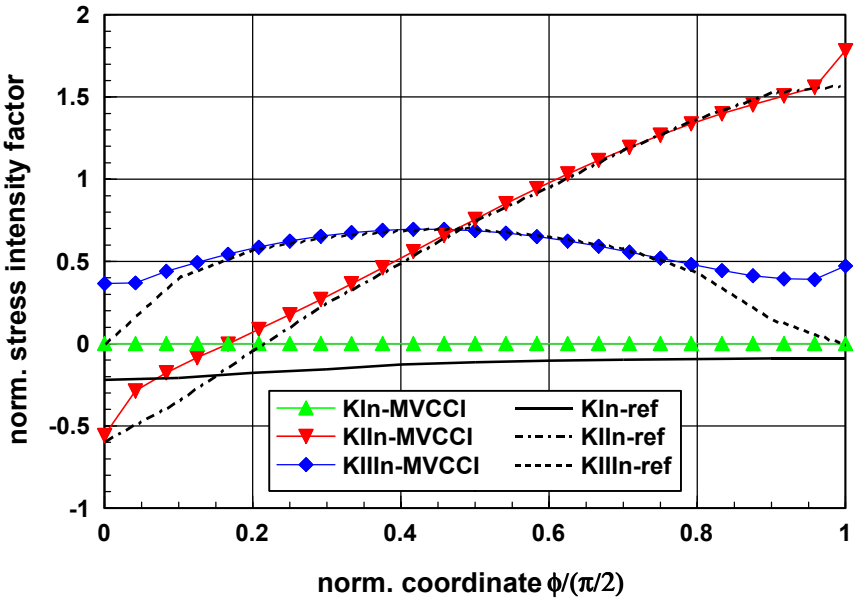

Figure 18: Norm. SIFs along the crack front of the QCCC specimen under shear loading

Three point bending (3PB) specimen

The last specimen type to be analysed in this investigation is the 3PB specimen as given in Fig.1d. Through the angled crack of γ=45 deg. primarily mode I and mode III loading conditions are generated along the crack front, which are given by a reference solution for a specimen of infinite thickness (Pook[20]), see Fig.20. For our specimen with a thickness of only t=20mm these values can no more be taken as reference data, but still the courses of $K_{In}(a,z/t)$ and $K_{IIn}(a,z/t)$, evaluated by the MVCCI method for this 3D case, show only reasonable deviations from the plane strain solution. But again a strong mode coupling effect is found between mode III and mode II, due to the global deformation behaviour of the specimen, resulting in values $K_{IIn}(a,z/t) > K_{IIIn}(z/t)$ adjacent to the crack front intersections at z/t=±0.5. That these results are not artificial or irrelevant can be seen from the deformation of the deformed FE model of the 3PB specimen in Fig.19, but more pronounced from the crack tip detail also shown

in Fig.19. Here the mesh behind the crack tip clearly show in-plane sliding displacements in addition to the opening and out-of-plane displacements, which are directly due to the three point bending configuration with the angled crack.

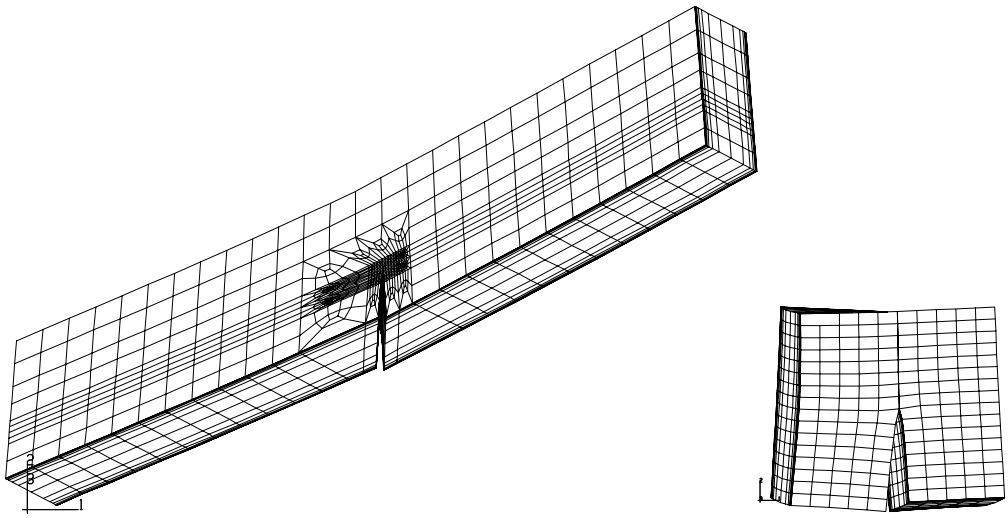

Figure 19: Deformed FE model of the 3PB specimen and crack surface detail
(6- and 8-node vol. el., w/Δa=96, Δa/a=0.031, Δa=0.625mm, Δt_{min}=0.1mm)

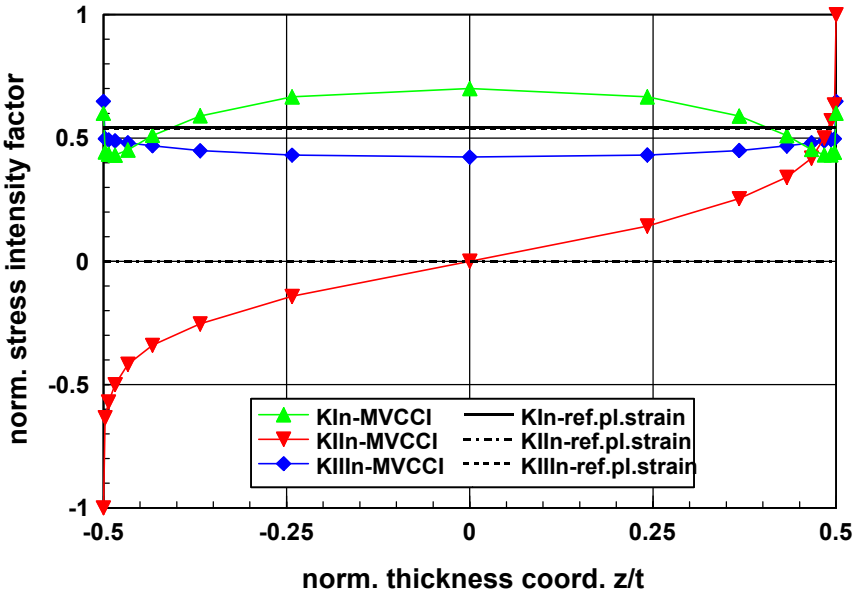

Figure 20: Norm. SIFs along the crack front of the 3PB specimen

In Fig.21 the strong impact of these effects on the development of further crack growth can be realised. In this case crack growth is no longer self similar and the crack kinks off from the original notch or crack plane, corresponding to the locally effective mixed mode ratio of mode I, II and III along the crack front. On a macro level this results in a crack twisting from its original plane into a new plane, where the crack will only experience mode I loading conditions with respect to the external loading of the specimen (Fig.21a). This global twisting behaviour of the originally plane crack is not fully understood, but a computational test performed by Dhondt[41] has shown that it can be modelled by considering only the variable mode I and II loading conditions along the crack front on the basis of the well known mixed mode I/II criteria (Richard[15]). On a meso level the crack surface of the twisted crack is not

smooth, in particular at the beginning of crack growth, but reveals narrow facets forming some angle with the direction of the overall crack growth (Fig.21b). This seems to be due to the superimposed mode III component generated by the external loading of the specimen with regard to the angled notch plane and has also been observed and discussed by Pook[43], Hull[44], but without considering the remarkable mode II portion of the locally effective crack front loading conditions. The governing relations concerning the local onset and direction of crack growth still have to be established for this rather complex case of 3D fracture. So far the 3PB specimen in combination with increasingly angled notch or crack planes seems to be suitable for this purpose.

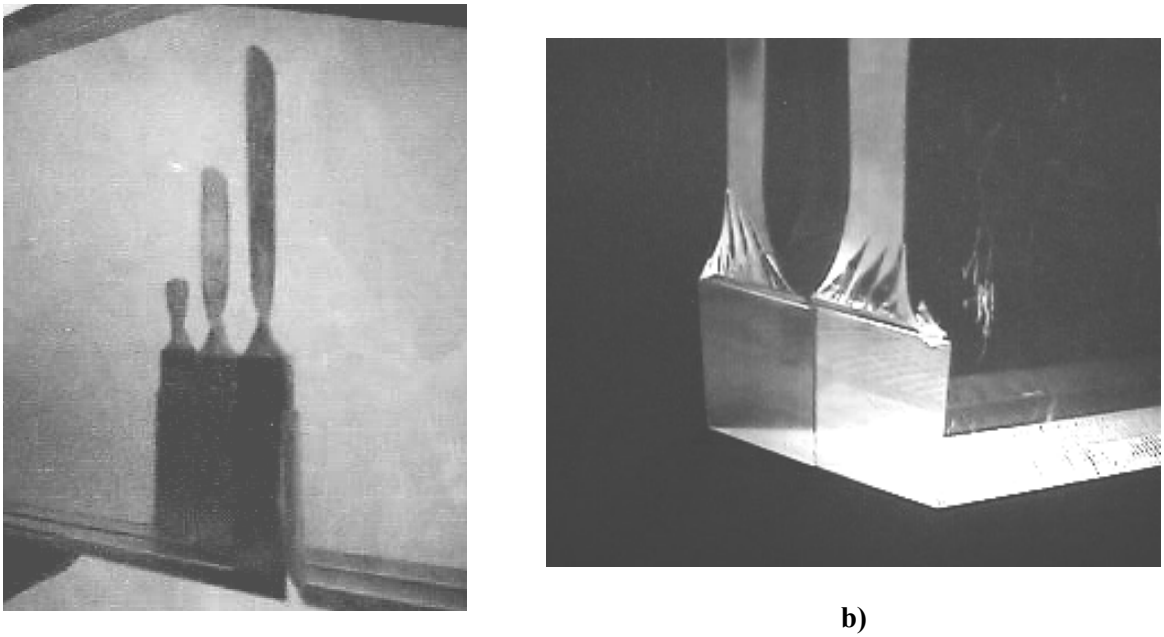

a) **b)**

Figure 21: Crack development in the SEN specimen with γ = 45 deg.
a) global twisting behaviour, **b)** local facet forming

SUMMARY AND CONCLUSIONS

In conclusion it can be stated that the accuracy and convergence of the Virtual Crack Closure Integral (VCCI) methods has fully been verified regarding the computational fracture analysis of 2D and 3D crack problems. For the 2D problems this has been done on the basis of a reference solution for the CCT specimen and in comparison to other methods. In the 3D cases (CCT, SEN, QCCC, 3PB) emphasis was on the analysis of mixed mode problems involving also local 3D and different mode coupling effects, in particular where a crack front intersects a free surface. It can be stated that the MVCCI results agree very well with the global behaviour of the reference solutions, but also remarkable deviations have been found where mode coupling effects seem not to be covered sufficiently by the solutions available from stress analysis handbooks or the literature. Also experimental evidence has been presented for the mode coupling effects analysed by the MVCCI method. Furthermore the MVCCI results have recently been strongly confirmed by findings from another approach, based on a different modelling technique and utilising singular quarter point volume elements.

REFERENCES

(1) Erdogan, F. and Sih, G. C.,On the crack extension in plates under plane loading and transverse shear. Journal of Basic Engineering, 85, 519-527, (1963)
(2) Williams, J. G. and Ewing, P. D., Fracture under complex stress- the angle crack problem. Int. J. Fract. 8, 441-446, (1972)

(3) Sih, G. C., Strain energy density applied to mixed mode crack problems. International Journal of Fracture, 10, 305-321, (1974)
(4) Hussain, M. A., Pu, S. I. and Underwood, J. H., Strain energy release rate for a crack under combined mode I and mode II. In Fracture Analysis, ASTM STP 560. American Society for Testing and Materials, Philadelphia, PA, pp. 2-28, (1974)
(5) Nuismer, R. J., An energy release rate criterion for mixed mode fracture. Int. J. Fracture 11, 245-250, (1975)
(6) Wu, C. H. Fracture under combined loads by maximum-energy-release-rate criterion, J. Appl. Mech. ASME. 45, 553-558 (1978)
(7) Palaniswamy, K. & Knauss, W. G., On the problem of crack extension in brittle solids under general loading, Mech. Today (Ed. S. Nemat-Nasser) Vol. 4. New York (1978)
(8) Cotterell, B. & Rice, J.R., Slightly curved or kinked cracks. Int. J. Fract. 16, 155-169, (1980)
(9) Sumi, Y., Nemat-Nasser, S. and Keer, L. M., On crack branching and curving in a finite body. Int. J. Fract. 21, 67-79,(1983). Erratum in Int. J. Fract. 24, 159 (1984)
(10) Amestoy, M., Bui, H. D. and Dang-Van, K., Analytic asymtotic solution of the kinked crack problem. In Advances in Fracture Research (Ed. D. Francois), 107-113, (1981)
(11) Leblond, J. B. and Amestoy, M., The stress intensity factors at the tip of a kinked and curved crack. In Advances in Fracture Research (Eds. K. Salama). Proc. of the 7th Int. Conf. on Fracture, Vol.3, 2339-2346, (1989)
(12) Richard, H.A., An new compact shear specimen. Int. J. Fracture 17, R105-R107, (1981)
(13) Richard, H.A. and Benitz, K., A loading device for the creation of mixed mode in fracture mechanics. Int. J. Fracture 22, R55-R58, (1983)
(14) Banks-Sills, L., Arcan, M. and Bui, H. D., Toward a Pure Shear Specimen for KIIC Determination, Int. J. Fracture, 22, R9-R14, (1983)
(15) Richard, H.A., Bruchvorhersagen bei überlagerter Normal- und Schubbeanspruchung von Rissen. VDI-Forschungsheft 631, VDI-Verlag, Düsseldorf, (1985)
(16) Tada, H. Paris, P., Irwin, G., The stress analysis of cracks handbook. Del Research Corporation, St. Luis, (1973)
(17) Rooke, D. P., Cartwright, D. J., Compendium of stress intensity factors. Her Majesty's Stationary Office, London, (1976)
(18) Murakami, Y. (Ed.), Stress Intensity Factors Handbook. Pergamon Press, Oxford, (1987)
(19) Isida, M, Analysis of Stress Intensity Factors for the Tension of the Centrally Cracked Strip with Stiffened Edges. Engng. Fract. Mech. 5, 647-665, (1973)
(20) Pook, L. P., A finite element analysis of the angle crack specimen. In Mixed-Mode Fatigue and Fracture, ESIS 14 (Eds. H. P. Rossmanith et al.). Mech. Engng. Publ., London, 285-302, (1993)
(21) Irwin, G. R., Analysis of stresses and strains near the end of a crack traversing a plate. J. of Applied Mechanics 24, 361 - 364, (1957)
(22) Irwin, G. R., Onset of fast crack propagation in high strength steel and aluminium alloys. In Sagamore Research Conference Proceedings, Vol. 2, 289 - 305, (1956)
(23) Rybicki, E.F., Kanninen, M.F.: A finite element calculation of stress intensity factors by a modified crack closure integral. Engng. Fract. Mech. 9, 931-938 (1977)
(24) Buchholz, F.-G., Improved Formulae for the Finite Element Calculation of the Strain Energy Release Rate by the Modified Crack Closure Integral Method. In Accuracy, Reliability and Training in FEM Technology (Ed. J. Robinson). Robinson and Associates, Dorset, 650-659, (1984)
(25) Krishnamurthy, T., Rammamurthy, T.S., Vijayakumar, K., Dattaguru, B., Modified Crack Closure Integral Method for Higher Order Finite Elements. In Finite Elements in Computational Mechanics (Ed. T. Kant), Pergamon Press, Oxford, 891-900, (1985)
(26) Raju, I.S., Calculation of strain energy release rates with higher order and singular finite elements. Engng. Fract. Mech. 28, 251-274, (1987)
(27) Sethuraman, R., Maiti, S.K., Finite element based computation of strain energy release rate by modified crack closure integral. Engng. Fract. Mech. 30, 227-231, (1988)
(28) Buchholz, F.-G., Schulte-Frankenfeld, N., Meiners, B., Fracture Analysis of Mixed-Mode Failure Processes in a 3D-Fibre/Matrix Composite Cylinder. In Proc. 6th Int. Conf. on Composite Materials, Vol.3 (Eds. Matthews et al), Elsevier Appl. Science Publ., London, 3.417-3.428, (1987)

(29) Buchholz, F.-G., Grebner, H., Dreyer, K.H., Krome, H., 2D- and 3D-Applications of the Improved and Generalized Modified Crack Closure Integral Method. In Comp. Mechanics 88, Vol. 1 (Eds. S.N. Atluri et al.), Springer Verl., New York, 14.i.1-14.i.4, (1988)
(30) Narayana, B. K., Krishnamurthy, T., Dattaguru, B., Ramamurthy, T.S., Vijay Kumar, K., Modified Crack Closure Interal for Three Dimensional Crack Problems. Paper pres. at Int. Conf. on Computational Engineering Science (ICES), Atlanta, GA, USA, (1988)
(31) Shivakumar, K.N., Tan, P.W., Newman, J.C.Jr., A Virtual Crack-Closure Technique for Calculating Stress Intensity Factors for Cracked Three Dimensional Bodies. Int. J. of Fracture 36, R43-R50, (1988)
(32) Buchholz, F.-G., Finite Element Analysis of a 3D Mixed-Mode Fracture Problem by Virtual Crack Closure Integral Methods. In Fracture Mechanics (Eds. A.V. Krishna Murthy, F.-G. Buchholz), Proc. of the Indo-German Workshop on Advances in Frature Mechanics, Indian Institute of Science, Bangalore, India, March 1994, Interline Publ., Bangalore, 7-12, (1994)
(33) Chan, S. K., Tuba, I. S. and Wilson, W. K., On the finite element method in linear fracture mechanics. Engng. Fracture Mech. 2, 1 - 17, (1970)
(34) Parks, D. M., A stiffness derivative finite element technique for determination of elastic crack tip stress intensity factors. Int. J. Fracture 10, 487 - 502, (1974)
(35) Hellen, T. K., On the method of virtual crack extension. Int. J. Num. Meth. Engng. 9, 187 - 208, (1975)
(36) Kuna, M., Konstruktion und Anwendung hybrider Rißspitzenelemente für dreidimensionale bruchmechanische Aufgaben, Technische Mechanik 3, 37-43, (1982)
(37) Nikishkov, G.P., Atluri, S.N., Calculation of Fracture Mechanics Parameters for an Arbitrary Three-Dimensional Crack by the Equivalent Domain Integral Method. Int. J. Num. Meth. Engng. 24, 1801-1821, (1987)
(38) Mi, Y. and Aliabadi, M. H., Three dimensional crack growth simulation using BEM. Computers and Structures 52, 871-878, (1994)
(39) Wawrzynek, P. A., Carter, B. J., Potyondy, D. O. and Ingraffea, A. R., A topological approach to modeling arbitrary crack propagation in 3D. In Diana Computational Mechanics‘94 (Eds. G. M. A. Kusters and M. A. N. Hendriks), Kluwer Academic, Dordrecht, 69-84, (1994)
(40) Dhondt, G., General behaviour of collapsed 8-node 2-D and 20-node 3-D isoparametric elements. Int. J. Num. Meth. Engng. 36, 1223-1243, (1993)
(41) Dhondt, G., Cutting of 3-D finite element mesh for automatic mode I crack propagation calculation. Int. J. Num. Meth. Engng. 42, 749-772, (1998)
(42) Buchholz, F.-G., Chergui, A., Dhondt, G., A comparison of SIF and SERR results with reference solutions regarding 3D and mode coupling effects for different specimens. In Fracture and Damage Mechanics 99 (Ed. M. H. Aliabadi), Dept.of Engng., Queen Mary and College, London, (1999)
(43) Pook, L.P., On the fatigue crack paths. Int. J. Fatigue 17, 5-13, (1995)
(44) Hull, D. The effect of mixed mode I/III on crack evolution in the brittle solids. Int. J. Fracture 70, 59-79, (1995)